Heliyon 9 (2023) e20088

Contents lists available at ScienceDirect

Heliyon

journal homepage: www.cell.com/heliyon

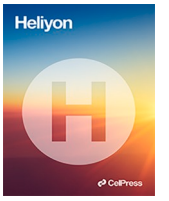

Modeling of land use/land cover dynamics using artificial neural network and cellular automata Markov chain algorithms in Goang watershed, Ethiopia

Getahun Sisay [a,*], Berehan Gesesse [b], Christine Fürst [c,d], Meseret Kassie [a], Belaynesh Kebede [a]

[a] Department of Geography and Environmental Studies, University of Gondar, P. O. Box 196, Gondar, Ethiopia
[b] Department of Remote Sensing, Entoto Observatory and Research Center, Space Science and Geospatial Institute, P.O.Box 33679, Addis Ababa, Ethiopia
[c] Department of Sustainable Landscape Development, Institute for Geosciences and Geography, Martin Luther University Halle-Wittenberg, Halle (Saale), Germany
[d] German Centre for Integrative Biodiversity Research (iDiv) Halle-Jena-Leipzig, Puschstraße 4, 04103, Leipzig, Germany

ARTICLE INFO

Keywords:
LULC
MLP neural network
CA-Markov
Remote sensing
Goang watershed
Ethiopia

ABSTRACT

Land Use/Land Cover (LULC) change has inhibited sustainable development for the last millennia by affecting climate, biological cycles, and ecosystem services and functions. In this regard, understanding the historical and future patterns of LULC change plays a crucial role in implementing effective natural resource management. This study aimed to model and characterize the spatio-temporal trajectories of landscape change between the 1984 and 2060 periods. The satellite image spectral information was segmented into seven LULC classes using a hybrid approach of image spectral recognition. The supervised classification technique of Support Vector Machine (SVM) was used to classify the satellite images, whilst the Land Change Modeler (LCM) Module in TerrSet software was used to assess the historical trend and future simulation of LULC dynamics. To predict future landscape changes, transition potential maps were generated using a Multi-layer Perceptron (MLP) neural network algorithm. The findings of the study demonstrated that the Goang Watershed has experienced significant LULC change since 1984. During the 1984–2001, 2001–2022, and 1984–2022 periods, farmland showed a dramatic increasing trend with 7.5 km^2/yr^{-1}, 110.3 km^2/yr^{-1}, and 64.3 km^2/yr^{-1}, respectively. A similar trend was also observed in built-up areas with 0.5 km^2/yr^{-1}, 3.2 km^2/yr^{-1}, and 2 km^2/yr^{-1}. The expansion of farmland and built-up area was at the expense of forest, shrubland, and grasslands. With a business-*as*-usual scenario, the extent of farmland will continue to increase between 2022 and 2060 while rapid reduction is expected by forest, shrubland, and grasslands. The alarming rate of farmland and built-up area expansion will put significant pressure on biodiversity and ecosystem services in the area. As a result, eco-friendly conservation approaches should be implemented as soon as possible to maintain ecosystem health and encourage sustainable development.

* Corresponding author.
E-mail address: getahunsisayteshager@gmail.com (G. Sisay).

https://doi.org/10.1016/j.heliyon.2023.e20088
Received 22 April 2023; Received in revised form 8 September 2023; Accepted 11 September 2023
Available online 16 September 2023

1. Introduction

List of acronyms

CA	Cellular Automata
DEM	Digital Elevation Model
ERDAS	Earth Resource Data Analysis System
ESA	European Space Agency
GIS	Geographic Information System
KIIs	Key Informant Interviews
KIs	Key Informants
LCM	Land Change Modeler
LULC	Land Use Land Cover
MC	Markov Chain
MLPNN	Multi-Layer Perceptron Neural Network
UNCCD	United Nations Convention to Combat Desertification
UNEP	United Nations Environmental Program
USGS	United States Geological Survey

Land use and land cover are inextricably linked but distinct concepts [1,2]. The former indicates human use of land attributes, which is largely a concern of social scientists, and the latter characterizes the physical and biological condition of the land, which is primarily a concern of natural scientists [2]. Land Use/Land Cover (LULC) change is an inevitable biophysical phenomenon caused by the nonlinear interaction between the natural environment and human activities, which has a profound impact on the Earth's energy balance, biogeochemical cycles, climate, biodiversity, ecosystem services, and the complex interaction of many factors [2–7].

Worldwide, changes in LULC have been defined by gains of agricultural land and built-up areas at the cost of forests which are mostly related to agricultural land expansion, deforestation, and urbanization [6,8,9]. For instance, between the 1960 and 2019 periods, almost a quarter of the global land surface has been considerably affected by LULC transformation, of which forest loss was the highest [10]. According to FAO [11], there was a 3% reduction in global forests between 1990 (4128 million ha) and 2015 (3999 million ha). A recent estimate by FAO and UNEP [12] also revealed the loss of 170 million ha of the world's forests between 1990 and 2020. These unforeseen changes in LULC frequently come with multiple environmental costs in different locations, which, when aggregated globally, substantially impact essential components of Earth's system functioning [1,4].

Although LULC transformations are a pervasive global environmental phenomenon that affects critical ecological functions, the rates and types of changes vary geographically [13]. For example, afforestation and farmland abandonment have increased forest cover by 2.208 million ha/yr^{-1} in temperate regions. In contrast, deforestation, cropland expansion, and urbanization have rapidly declined forests (5.52 million ha/y^{-1}) in tropical areas [10,14]. The variation in the trends of LULC transformation among regions partly reflects the differences in land management practices, policies, weak enforcement, and the shifts in land use demands [5,6,8,15].

In Ethiopia, uncontrollable changes in LULC are more common mainly due to the changes in agricultural practices, unprecedented population growth, climate variability, and improper land resource utilization [16,17]. Recent studies in the country have indicated major changes in LULC as a result of the significant increase of cultivated land at the expense of forests, vegetation, grassland, and wetlands [18–23]. Some studies, however, have reported the encouraging increasing trends of forest cover and concomitant reduction of farmland, which mainly coincides with the expansion of plantations, and the shift from cropland to agroforestry-based farming [24–27]. According to Regasa et al. [28], the observed nonlinear pattern of LULC transformation in the country is primarily due to the complex and dynamic driving forces dependent on sustainable land management activities, environmental history, and livelihood, which necessitates time and location-specific research.

The Goang watershed has rich biodiversity due to its diversified agroecological systems [29]. It is home to ecologically and economically important forest ecosystems, including *Boswellia papyrifera* (Del.) Hochst species, renowned for the production of frankincense or *gum olibanum*, and myrrh products [29,30]. Though these forest species are vital for economic growth and are thought to have an important role in desertification control [31], they have been converted due to the changing socio-economic conditions, resettlement-induced slash-and-burn farming, ranching, and expansion of large-scale commercial farming [29,32]. Increasing human activity in the area promotes deforestation which poses far-reaching negative implications on soil quality, biodiversity, and climate [32]. Zewdie et al. [3] also argued that northwest Ethiopia along with the Sudan border occasionally experiences haze clouds during dry seasons, which may be attributed to the deterioration of the local natural vegetation. Despite its considerable ecological value and significant human strain, the Goang watershed has received less attention and is poorly recorded in scientific studies in comparison to other regions of Ethiopia.

Few studies have been carried out to assess the spatiotemporal patterns of LULC change near the study area [33,34]. However, updated information that takes into account the historical trends, current status, and future prediction of LULC change for the Goang watershed is still lacking. Furthermore, the evaluation of the dynamics of LULC has been done elsewhere in Ethiopia and abroad [13, 14,35–38]. However, most of them used Cellular Automata (CA) and Markov Chain (MC) approaches and they did not consider the

explanatory power of the drivers of LULC change in simulating the future changes.

The UNCCD secretariat identified LULC data as a crucial indicator for documenting land degradation and evaluating the status of land degradation neutrality [39]. This is because knowledge of the spatiotemporal variations in LULC provides a preliminary indication of the loss and restoration of land to help plan efficient land management strategies [40]. Thus, using GIS and remote sensing technologies combined with spatially explicit models is of fundamental importance to quantify the historical and future trends of LULC transformations [41]. So far, a variety of landscape change modeling techniques have been used, including but not limited to CA [35], MC [42], Multi-Layer Perceptron (MLP) neural networks [19,41], Similarity-Weighted Instance-based Machine Learning (SimWeight) [43], and Logistic Regression [44].

The MC model is a stochastic modeling approach and is effective for monitoring temporal changes in landscape patterns depending on transitional matrices [41]. However, they are unable to simulate the geographically distributed landscape changes [13]. On the contrary, the CA model is capable of predicting the geographical distribution of landscape patterns but it is unable to predict temporal changes [45]. In this instance, many authors suggest a hybrid of CA and MC to preserve the benefits and overcome the limitations of the two models [38,46]. Nonetheless, these models fail to account for the explanatory power of the driver variables in simulating LULC change over time [19]. As a result of recent breakthroughs in Artificial Intelligence (AI), Artificial Neural Networks (ANN) and CA-MC have been integrated to combine the capabilities of each technique [47]. Compared with SimWeight and Logistic Regression model, the MLP neural network outperforms well when it comes to simulating landscape changes, especially when there are nonlinear interactions between LULC and for modeling many transition types simultaneously [48]. As a result, this study was carried out utilizing GIS, remote sensing, and MLP-CA-MC models to achieve the following objectives:

1. Explore the spatiotemporal dynamics of LULC in the Goang watershed from 1984 to 2022.
2. Predict future LULC changes from 2022 to 2060 using an MLP and CAMC modeling approach.

The findings of this study are expected to provide vital insights to relevant organizations for the development of effective and sustainable conservation strategies, aimed at preserving the environment and safeguarding its ecological integrity.

2. Methods and materials

2.1. Study area

Goang watershed is part of the western drainage system in northwestern Ethiopia in the Amhara Regional State. It is part of of the Tekeze River basin, which drains westward, ultimately joining the Nile in Sudan and ending at the Mediterranean Sea. Spatially, it extends from 12°30′00″ to 13°20′00″ North of latitude and 36°20′00″ to 37°20′00″ East of longitude (Fig. 1).

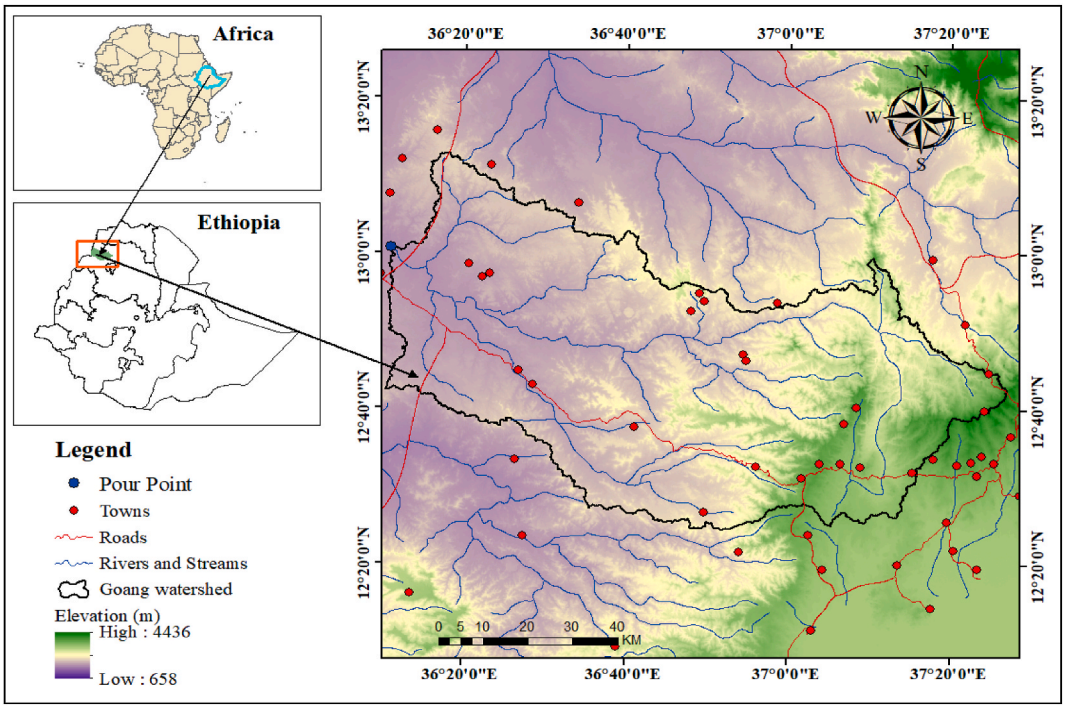

Fig. 1. Location map of the Study area.

Based on Hurni [49] traditional agroecological classification system, the vast majority of the study area is *Kolla* (lowland) (78%) followed by *Woyina dega* (sub-humid highlands) (21.16%) and the minor area is *Dega* (humid highlands). The watershed has the lowest elevation of 658 m around the lowlands of the Metema and the highest elevation of 2700 m in the districts of Chilga, Lay Armachiho, and Denbia. The study area is characterized by unimodal rainfall, and the rainy months extend from June to the end of September. However, most of the rain is received during July and August [50]. The annual mean minimum and maximum temperatures in the watershed vary from 19.4 °C to 35.8 °C in Metema and 13.5 °C–24.3 °C in Ayikel station, respectively.

The study area is abundant in many vegetation species and forest resources. For instance, the dry evergreen montane forest is predominantly found between 1500 and 2700 m above mean sea level [51]. However, these forest resources are the most fragmented due to human encroachment and conversion to cereal-based mixed agriculture [51]. Combretum-Terminalia deciduous forest, an extension of the Sudano-Sahelian vegetation formation is primarily found in the lowland sections of the study area [29]. These forest resources dominantly contain economically important forest species of *Boswellia Papyrifera* which is famous for producing Frankincense [29], primarily found on rocky and steep hillsides [31]. However, due to livestock grazing, browsing, trampling, deforestation, and climate anomalies, it faces threats to its regeneration status [29,52].

2.2. Datasets and sources

We collected spatial and non-spatial data from both primary and secondary sources. Key Informant Interviews (KIIs), direct field observation, and GPS-based ground truth datasets were primary data sources, while secondary data were acquired from various spatial data providers, published articles, and governmental reports.

KIIs were carried out to determine the major drivers of LULC change in the study area. Thus, Key informant interviewees including local farmers, community leaders, government officials, and environmental experts with specialized expertise and experience associated with the major driving forces of LULC change in the Goang watershed, were selected through a random sampling technique. A total of 36 key informants (KIs): six development agents, two agriculture and rural development office experts, twenty-five elderly household heads, and three environmental protection, land administration, and use authority office experts were interviewed.

2.2.1. Sources of spatial data

Landsat Thematic Mapper (TM) and Enhanced Thematic Mapper Plus (ETM^{+}) satellite images were obtained from the United States Geological Survey (USGS) website while Sentinel-2A images were obtained from the European Space Agency (ESA) through the Copernicus hub. The images had a spatial resolution of 30 m for Landsat TM and ETM^{+} and 10 m for Sentinel 2A. Satellite images scanned in November were considered to assess LULC changes (Table 1). The reason for choosing November mosaics is that this month is typically associated with the end of the rainy season and the beginning of the dry season in the Northwest Amhara Region. During this period, crops are typically harvested, and the vegetation cover is at its maximum. This makes it easier to discriminate between different land cover features, as they have varying reflectance values that can be more easily distinguished from each other. Moreover, selecting November mosaics for the analysis was based on the recommendation from previous literature, specifically, Mekonnen et al. [30], who advised using satellite images obtained in November for the northwestern and northern lowlands, and in January for the rest of the Amhara region. This recommendation is based on the fact that November is typically associated with the end of the rainy season in the western and northern lowlands, which makes it an ideal time to assess forest resources in those areas.

High-Resolution (HR) Advanced Land Observing Satellite-Phased Array-Type L-Band Synthetic Aperture Radar (ALOS-PALSAR), Radiometrically Terrain Corrected (RTC) DEM with 12.5 m*12.5 m resolution was used to delineate the study area's watershed boundary and to prepare slope and elevation maps. This data was acquired from the Atlanta Satellite Facility (https://asf.alaska.edu/) [53]. Road networks, towns, and village maps were obtained from the Federal Democratic Republic of Ethiopia Ministry of Mines while a population density map (People/Km^2) with a spatial resolution of 30 arc seconds was acquired from the Worldpop database (www.worldpop.org) [54].

2.2.2. Ground data sampling

Ground data were sampled using a stratified random sampling technique. This approach involves dividing the study area into strata based on LULC classes and randomly selecting a predetermined number of sample points within each stratum [55]. A total of 1810

Table 1
Details of satellite images used for LULC change analysis.

Satellite	Dataset ID	Date acquired	Sensor	Data format	Cell size
Landsat 5	LTO5L1RP170051198411292020091802T1	1984/11/29	TM[a]	Geo Tiff	30 m
Landsat 7	LE07L1TP170051200111252020091702T1	2001/11/25	ETM+[b]	Geo Tiff	30 m
Sentinel 2	T37PBQ20221118T074931	2022/11/18	MSI[c]	Jpeg 2000	10 m
	T37PCP20221117T075211	2022/11/17	MSI	Jpeg 2000	10 m
	T37PBP20221117T075211	2022/11/17	MSI	Jpeg 2000	10 m
	T37PCQ20221131T075211	2022/11/31	MSI	Jpeg 2000	10 m
	T37PBQ20221118T075211	2022/11/18	MSI	Jpeg 2000	10 m

[a] TM:Thematic Mapper.
[b] TM^{+}: Thematic Mapper Plus.
[c] MSI: Multispectral Instrument.

ground truth datasets were collected using this method; 1200 were used for image classification, and 610 points were used for accuracy assessment.

Various methods were used to collect the ground data, including field-level GPS data collection and Google Earth images. Google Earth images were mainly used to supplement the GPS data, to get additional information on LULC classes, and to aid reference data collection in locations where GPS field data collection was impossible.

It is crucial to account for the dynamic nature of surface phenology during reference data collection for LULC change analysis because changes in vegetation and other surface features may cause fluctuations in reflectance values acquired by remote sensing sensors [21]. In this regard, ground data were collected close to the acquisition date of the remotely sensed imagery in order to ensure that the ground data accurately represents the current state of the surface, which can help improve the accuracy of LULC analysis.

2.3. Methods of data analysis

2.3.1. Image pre-processing

The Landsat level-1 products are already geometrically corrected, radiometrically calibrated, and orthorectified using ground control points, and DEM by the data provider [56]. However, preprocessing operations, particularly image enhancement, layer stacking, mosaicking and pixel size resampling were done for raw satellite images. Image enhancement was applied for the satellite images to increase visual discrimination between features. At the same time, layer stacking was done to convert multiple single-band images into a single multi-spectral image [57]. During the layer-stacking process, bands 1–5 and 7 were considered for Landsat 5TM and ETM^{+} images while bands 2–4 and 8 were used for Sentinel 2A satellite images [19,21]. The Sentinel 2A image swath width was unable to cover the whole study area boundary. Hence, separate Sentinel-2A images, which are composed of 100 km × 100 km tiles were combined using mosaic tools in ERDAS IMAGINE 2014 to get a composite image with complete coverage of the study area.

Resampling was done for satellite images to ensure that they have the same spatial resolution and projection, which is required for conducting a reliable analysis of LULC change [58]. Hence, the 10-m resolution of Sentinel 2 images was resampled to a 30-m

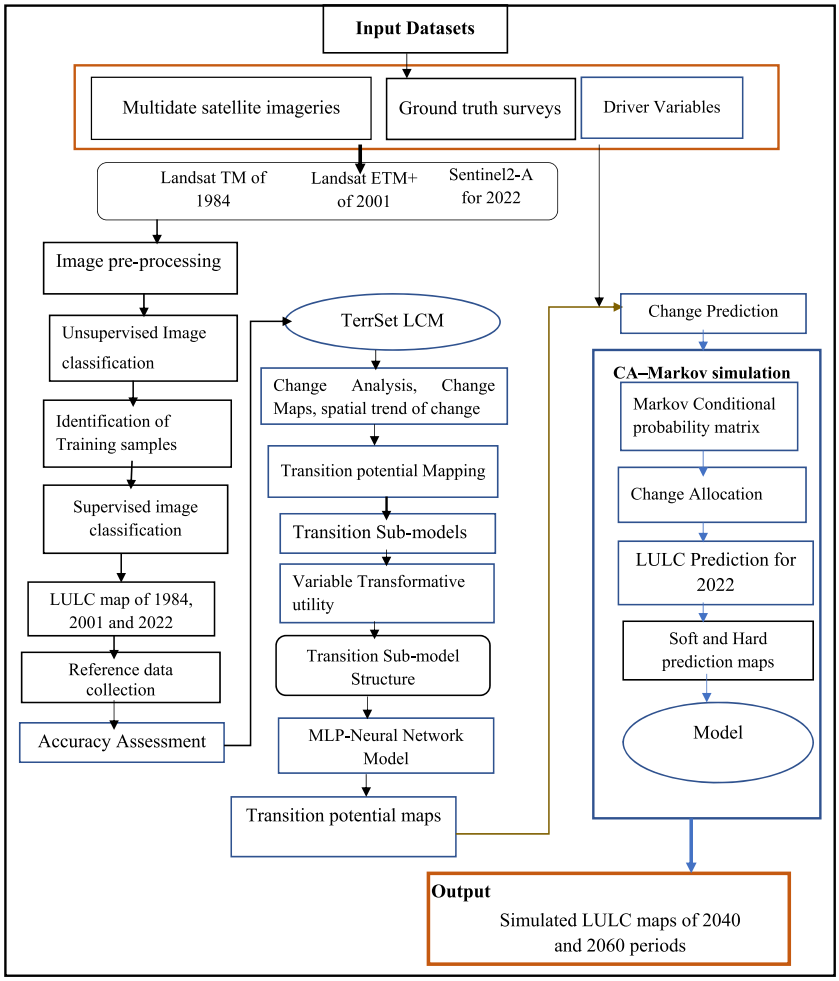

Fig. 2. General workflow of the study.

resolution using the nearest neighbor method. This method assigns the nearest pixel value from the original image to the resampled pixel without any interpolation, which preserves the original spatial characteristics of the image to a greater extent than bilinear interpolation and cubic convolution [58]. The resampling process was carefully conducted to ensure that the spatial features of the images were preserved and that the resampled images accurately represented the original images. We also performed quality control checks to ensure that the resampled images were free of any distortions that might have been introduced during the resampling process.

2.3.2. LULC classification

Landsat satellite images of 1984, 2001, and Sentinel-2A for 2022 were used to analyze the patterns of LULC transformations (Fig. 2). The year 1984 was purposely selected as the starting study period because this year marks a significant period in Ethiopia's history, as it was the year when the then military government started a large-scale resettlement program to address the country's growing population and land scarcity issues [59]. This program led to significant changes in LULC patterns in many parts of the country, including our study area. The availability of satellite images for 1984 also provides a unique opportunity to study the baseline conditions of the study area before the resettlement program and other major land use changes occurred.

Satellite images were automatically classified into seven categories to derive LULC information classes (Table 2). Thus, hybrid approaches of image classification were employed as they provide an acceptable result, particularly in locations with varied biophysical compositions [60]. Initially, unsupervised classification was utilized to identify commonly occurring distinctive spectral clusters that represent major LULC classes using the Iterative Self-Organizing Data Analysis Technique (ISODATA) [56]. Based on actual field-level data and the use of Google Earth images, the resulting information class names were manually tagged [60]. Google Earth images mainly facilitated LULC class signature collection by connecting ERDAS IMAGINE 2014 to the Google Earth time slider tool. This method helped distinguish LULC types with identical reflectance values. Lastly, the Support Vector Machine (SVM) algorithm of the supervised classification method was used as it has a higher accuracy for images derived from spatially complex land cover categories [61]. During the image classification procedure, at least 50 training sample locations for each LULC class were gathered as per the recommendation of Congalton and Green [62].

2.3.3. Accuracy assessment

According to Foody [63], the output of the quality of the classified images must be evaluated through accuracy assessment techniques before beginning post-classification analysis. Accordingly, we evaluated the performance of the classification algorithm by comparing the classification results from the satellite imageries to the ground truth data collected through the stratified random sampling method. Specifically, 610 ground truth points were randomly selected, and the classification results were compared to the LULC classes observed at these points. The accuracy of the classification was then quantified using a range of metrics, such as Overall Accuracy (OA), User's Accuracy (UA), Producer's Accuracy (PA), and Kappa coefficient using Eqs. (1)–(4), respectively following Foody [63].

$$\mathrm{OA} = \frac{\sum_{i=1}^{r} D_{ii}}{N} \tag{1}$$

$$\mathrm{UA} = \frac{\sum D_{ij}}{x_{+i}} \tag{2}$$

$$\mathrm{PA} = \frac{\sum D_{ij}}{x_{i+}} \tag{3}$$

$$K_{hat} = \frac{N\sum_{i=1}^{r} X_{ii} - \sum_{i=1}^{r}(X_{i+} * X_{+i})}{N^2 - \sum_{i=1}^{r}(X_{i+} * X_{+i})} \tag{4}$$

Where D_{ii} is the number of correctly classified sample pixels, N is total samples, D_{ij} is the number of correctly classified pixels in row i, D_{ij} is the number of correctly classified pixels in column j, r is the number of rows in the matrix; xii is the number of pixels in row i and column i; x_{i+} and x_{+i} are the marginal totals of row i and column i, respectively; K_{hat} is kappa coefficient, $N\sum_{i=1}^{r} X_{ii}$ is observed accuracy, and $\sum_{i=1}^{r}(X_{i+} * X_{+i})$ is chance accuracy.

Table 2
Identified LULC classes and their description [42,57].

	LULC type	Description
1	Forest	Areas covered with dense trees formed nearly closed canopy cover of >10%, 5 m in height, and 0.5 ha in area
2	Shrublands	Areas covered by sparsely distributed bush trees and grasses.
3	Farmland	Areas of land used for both perineal and annual crops
4	Bare land	Areas with no vegetation cover due to erosion, overgrazing, or mismanagement.
5	Water	Surface water, including rivers and streams
6	Built-up area	Areas covered by urban and rural settlements and impervious roads
7	Grassland	Areas covered with grass used for grazing.

2.3.4. LULC change analysis

The changes in LULC were assessed using TerrSet software using the LCM tool. To measure and depict LULC over time, LCM employs a number of statistical and spatial models [48]. The tool offers a variety of features, including change analysis, trend analysis, transition probability analysis, and spatial pattern analysis. Accordingly, LULC transitional matrices which depict persistence, gains, losses, and exchanges of LULC cover were produced using a "change analysis" panel. The columns in the matrix correspond to the later periods (newer LULC classes), whereas the rows in the matrix indicate the earlier periods (old land cover). The bold diagonals in the matrix show classes that remained the same or underwent no change during the study periods, whereas the off diagonals show LULC classes that were switched to another class.

The extent of change of LULC across time was calculated using percent (Eq. (5)) and annual rates of change (Eq. (6)) following a method derived from Refs. [21,57].

$$R\Delta(\%) = \left(\frac{G_2 - G_1}{G_1}\right) * 100 \tag{5}$$

$$\text{Rates of change } \left(\text{Km}^2 \,/\, \text{year}\right) = \left(\frac{G2 - G1}{S}\right) \tag{6}$$

where R (%) denotes the percentage change in one type of LULC between the first (G_1) and second (G_2) periods of a LULC class in Km^2, and S represents the time interval between G_1 and G_2 in a study year.

2.3.5. Prediction of future LULC change and spatial driver variables

A combination of MLP neural networks, CA, and MC algorithms were utilized in TerrSet software LCM tools to project future LULC scenarios. The TerrSet LCM creates a predictive model based on observed trends in previous LULC data using a combination of statistical and machine-learning techniques [48]. As a result, transition potential maps were constructed to predict future LULC changes utilizing the "transition potential" tab in the LCM modeling tools. Transition Potential Modelling (TPM) is a helpful tool in environmental management and planning because it allows for the assessment of the likelihood of various land use transitions occurring in a certain location [25,64]. The goal of TPM is to identify areas with high potential for LULC change, which can be targeted for conservation or land use planning efforts [38,47]. The model takes into account several factors that influence LULC change and employs these elements to generate transition potential maps [48]. To develop transition potential maps, LULCs that experience considerable transformation and are assumed to have the same underlying driver variables between two study periods were grouped into a series of experimentally evaluated transition sub-models. After specifying the sub-models, the driver variables were added to the model as a static and dynamic component using the "Transition Sub-Model Structure" panel.

Spatial driver variables are the various biophysical, socio-economic, and demographic factors that influence LULC change in a specific area [42]. These variables may include both natural and human factors [41]. However, for this study, population density, elevation, slope, evidence likelihood, and proximity parameters like distance from roads, towns, and rivers were considered (Fig. 6). The selection of these variables was based on the review of various literature and considering the specific context of the study area. The significance of the driver variables during the future LULC change projection was tested using Cramer's V coefficient. The Cramer's V coefficient is a statistical measure of the degree of association between two categorical variables [19,25]. The coefficient ranges from 0 to 1, with higher values suggesting a stronger relationship between the two variables [42].

The TerrSet LCM includes three popular machine learning algorithms that can be used for LULC change modeling: Similarity-Weighted Instance-Based Machine Learning (SimWeight), Logistic Regression, and Multi-Layer Perceptron (MLP) neural network [48]. The advantage of MLP neural networks over SimWeight and Logistic Regression is their ability to learn complex data patterns and relationships [42,48]. After developing transition potential maps, LULC change prediction was performed using stochastic modeling algorithms of CA-MC. The CA model simulates the spatial dynamics of LULC changes, while the MC model estimates the probabilities of transition between different land use categories based on historical patterns [38,65,66]. The CA model simulates the changes in LULC over time by applying a set of rules that determine how a cell can change based on its current state and it's neighboring as expressed by Eq. (9) [14,38]. The MC model on the other hand is based on a transition probability matrix that describes the probability of a pixel changing from one LULC class to another over a given time interval. The model can be represented by the following equations (Eq. (7) and (8)) Leta et al. [42]:

$$S(t+1) = Tij \; x \; S(t) \tag{7}$$

$$\text{T}ij = \begin{bmatrix} \text{T}11 & \text{T}12 & \ldots & \text{T}1n \\ T21 & T2 & \ldots & T2n \\ \vdots & \vdots & \ldots & \vdots \\ \text{T}n1 & \text{T}n2 & \ldots & \text{T}nn \end{bmatrix} (0 \le \rho\text{ij} \le 1) \tag{8}$$

$$M(t+1) = F(L(t), N) \tag{9}$$

where: S(t+1) is the predicted land cover map at time t+1, Tij is the transition probability matrix that describes the probability of a pixel changing from one LULC class (i) to another (j), S(t) is the initial land cover map at time t, M(t+1) is the predicted LULC map at time t+1, L(t) is the initial land cover map at time t, N is the neighborhood of each cell, which includes the adjacent cells that influence

its behavior, F is the transition function that determines how each cell in the grid will change based on the land cover class of its neighbors.

The "Change allocation" tool in TerrSet LCM was used to build two simulated maps for the year 2022, i.e., soft and hard prediction maps, used to predict future scenarios of LULC change. A hard prediction map is a binary map that depicts the projected land cover classes for a certain time interval; each pixel in the map is assigned to one land cover class, based on the model's prediction [48]. A soft prediction map, on the other hand, is a continuous map that provides a probability value to each pixel, indicating the chance of it belonging to a specific land cover class. The values typically range from 0 to 1, with lower values indicating a lower vulnerability to change and higher values indicating a higher vulnerability to change [19].

2.3.6. Model validation

Model validation is an important step in the TPM process to ensure the accuracy and reliability of the models [48]. In this study validation process includes testing the model's performance using historical data and comparing the predicted results to the actual observed results [47]. This helps to assess the model's accuracy and reliability in predicting LULC change. The method we used involved comparing the predicted 2022 LULC map to observed maps of 2022 using the validation tab in the LCM module. Once a model has been validated, we predicted the future LULC changes for the 2040 and 2060 periods.

2.3.7. Sensitivity and performance of MLP model

The MLP model available in LCM was used to build the transition potential map after evaluating the power of explanatory variables. To do this MLP starts the automatic training process by selecting a random sample of cells that transitioned between time1 (2001) and time 2 (2022) LULC classes [48]. Hence, the sample size per class was drawn from the examples of transitioned and persisted classes for the training and validation process. The MLP by default assigns 10,000 sample sizes per class. However, in this study, 1656 samples per LULC class were used, of which 50% was used for training and 50% for testing with 10,000 iterations (Table 6). The MLP evaluated the predictive power of the driving variables by looking at variations in skill measure and accuracy rate [48]. As a result, three alternative model sensitivity analysis methodologies were employed to evaluate the variations in skill measure and accuracy rate. To determine which independent variable has the biggest impact on future LULC predictions, the first approach (forcing one independent variable to be constant) holds all other variables constant [48]. The second strategy is holding all independent variables constant, except one to collect data on each variable. Following this method, training begins with all factors involved, then each variable is forced to remain constant to examine the impact of removing each variable on the accuracy rate and skill measure. The skill measure extends from −1 to +1, with a value of −1 signifying skills that are more valuable than guessing and a value of 0 denoting no skills [47].

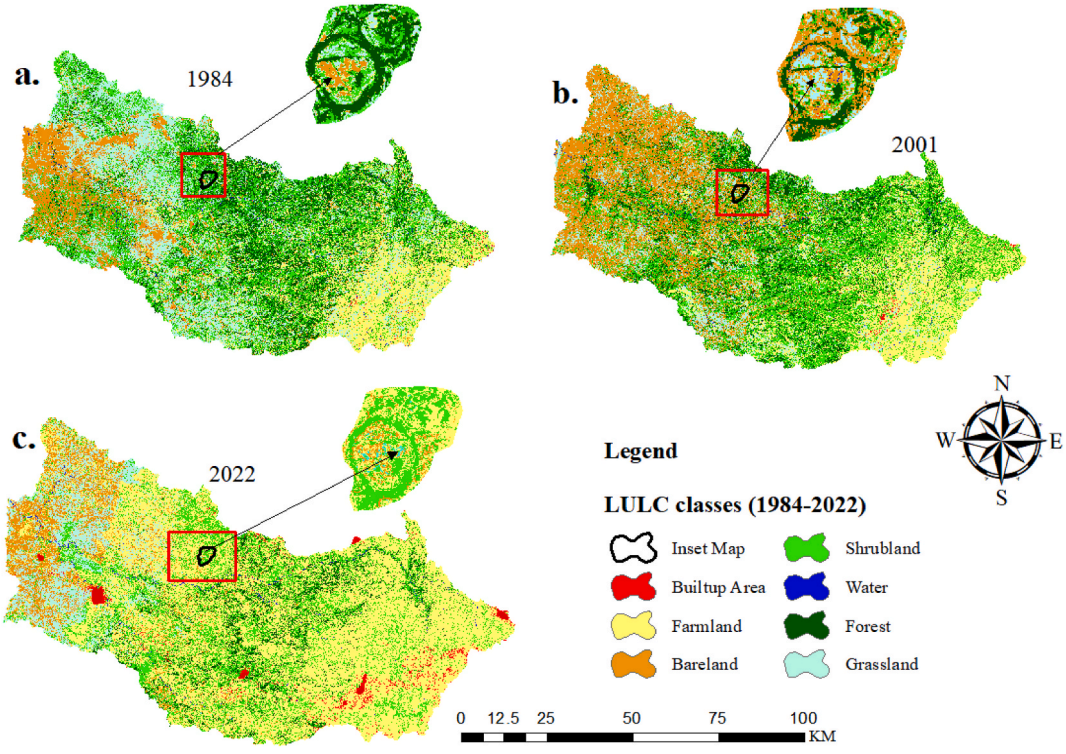

Fig. 3. Classified LULC map of 1984 (**a**), 2001 (**b**), and 2022 (**c**).

3. Results

3.1. Accuracy assessment and LULC classification result

The error matrix (Table A1-3) depicts the accuracy of the classified satellite imagery. The study found Kappa coefficient values of 84.68%, 87.17%, and 91.76% for 1984, 2001, and 2022, respectively. Additionally, the overall accuracy results of the classified images were determined to be 86.88%, 89.01%, and 92.95% for the years 1984, 2001, and 2022, respectively. Following the verification of the accuracy assessment results, the spatiotemporal patterns of LULC transformation were assessed, and the results showed that during the 1984 period, shrublands (31%), grassland (23%), farmland (19.4%), and forests (14.5%) covered a sizable portion of the watershed (Fig. 3). Shrublands continued to be the leading LULC class in 2001, accounting for 31.5% of the total area, followed by farming (21.3%), bare land (21.8%), forest (13.3%), and grassland (11.25%). Grassland experienced the highest loss (23.02%) in 1984 vs. 11% in 2001, mainly attributable to increased farmland and barren land. Farmland expanded quickly, taking 56% of the study area in 2022, whereas forest, grassland, and shrubland saw significant area losses, which shared 4.8%, 8.82%, and 20.7%, respectively.

Significant spatiotemporal discrepancies in the trends and magnitude of LULC change have been observed across different agro-ecological zones. For instance, in 1984, a significant portion of farmland was spatially dispersed in the *Weyinadega* (midland) agro-ecological zone. In contrast, a considerable area of forest and shrubland were primarily distributed in the lowland (*kolla*), followed by *Weyinadega* (midland). However, between 2001 and 2022, farmland increased dramatically in nearly all agroecology at the expense of forests, grasslands, and shrublands.

3.2. Rates of LULC conversions between 1984 and 2022

Farmland increased at an averagerate of 7.517 km^2/yr^{-1}, 110.2 km^2/yr^{-1}, and 64.26 km^2/yr^{-1} across the three periods (1984–2001, 2001–2022, and 1984–2022). Similarly, built-up areas increased by 0.5 km^2/yr^{-1}, 3.17 km^2/yr^{-1}, and 2 km^2/yr^{-1} between 1984 and 2001, 2001–2022, and 1984–2022, respectively (Table 3). On the other hand, forest, shrubland, and grassland areas decreased at annual rates of 16.95 km^2 ha/yr^{-1}, 18.76 km^2/yr^{-1}, and 40.16 km^2/yr^{-1}, respectively, over similar periods.

Although forest cover declined steadily throughout the study periods, the period between 2001 and 2022 had faster rates of forest cover loss than the period between 1984 and 2001 (Table 3 and Fig. 4).

3.3. Percentage change and contributors to net change by each LULC type

The gains and losses analysis results indicate significant changes in LULC during the three time periods analyzed. Farmland expanded by 2604.41 km^2 between 2001 and 2022, with gains mostly from shrubland (1259.21 km^2), grassland (421.4 km^2), and forest (331.63 km^2). We observed rapid and substantial loss of forest, grassland, and shrubland, with reductions of 66.67%, 61.66%, and 34.55%, respectively, between 1984 and 2022. In contrast, built-up areas and farmland consistently and dramatically increased by 380.96% and 188.9%, respectively, over the same period (Table 4 and Fig. 4). Though major forest-covered areas have shown drastic reduction during the studied periods, non-forest area conversion to forest and shrubland was also seen mainly in the midland and highland parts of the study area.

The contribution of each LULC class to the observed change was investigated. During 1984–2001, bare land, farmland, and shrubland were the primary negative contributors to net change experienced by forests. Similarly, from 1984 to 2022, farmland was the most significant negative contributor to net change experienced by all LULC classes except built-up areas (Fig. 5**b**, **d**, **e,** and **f**). Considerable farmland areas were also converted to built-up areas with net change of 28.6 km^2 in Fig. 5a.

3.4. MLP skill measure result

The MLP model training obtained an accuracy rate of 87.23% (Table 5), which is beyond the acceptable percentage of rate of

Table 3
Areal coverage of LULC, percent, and rates of changes between 1984 and 2022.

LULC classes	Study periods						Change					
	1984		2001		2022		1984–2001		2001–2022		1984–2022	
	Km^2	%	Km^2	%	Km^2	%	%	Rate	%	Rate	%	Rate
Bare land	766.07	11.5	1455.11	21.83	548.4	8.23	89.94	40.53	−62.31	−43.17	−28.41	−5.73
Built-up area	19.8	0.3	28.46	0.42	95.23	1.43	43.73	0.5	94.98	3.18	380.96	1.98
Farmland	1293.1	19.4	1420.9	21.31	3735.77	56.04	9.88	7.52	162.91	110.23	188.9	64.3
Forest	966.6	14.5	886	13.3	322.1	4.83	−8.33	−4.74	−63.64	−26.85	−66.67	−16.96
Grassland	1534.8	23.02	749.34	11.24	588.35	8.82	−51.17	−46.2	−21.48	−7.66	−61.66	−24.9
Shrubland	2063.93	30.96	2103.71	31.56	1350.86	20.26	1.93	2.34	−35.8	−35.85	−34.55	−18.76
Water	21.12	0.31	21.9	0.33	24.71	0.37	3.7	0.045	12.83	0.133	17	0.09
Total	6665.42	100	6665.42	100	6665.42	100						

Rate*: The annual rate of LULC change (Km^2/year).

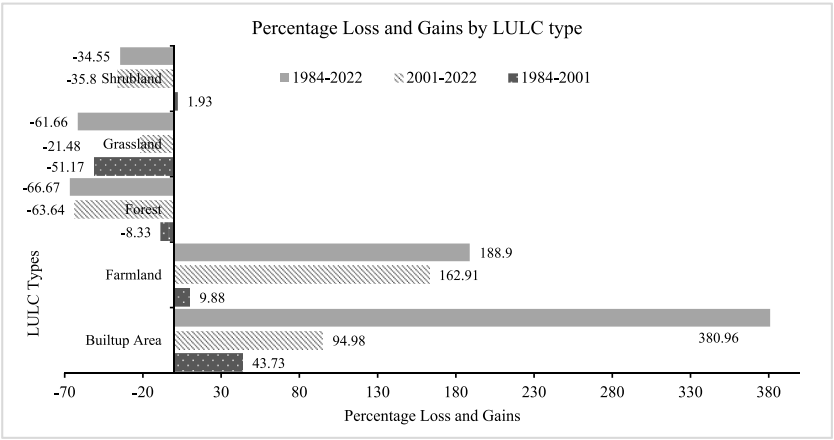

Fig. 4. Percentage Gains and losses by LULC class.

Table 4
Transition area matrix between 1984 and 2022 periods.

To	2001	Bare land	Built-up area	Farmland	Forest	Grassland	Shrubland	Water	Total	Loss
From 1984	Bare land	**373.85**	2.28	73.9	62.7	119.38	129.54	4.237	765.9	392.04
	Built-up area	1.31	**1.056**	7.7	0.85	3.734	5.026	0.074	19.74	18.691
	Farmland	94	10.3	**643.51**	92.4	68.72	379.3	4.123	1292.33	648.823
	Forest	77.55	2.16	94.979	**448.44**	11.406	331.24	0.63	966.41	517.97
	Grassland	504	6.95	276.5	48.15	**430.51**	266.04	3.5	1535.66	1105.15
	Shrubland	400.01	5.61	318.45	232	115.4	**991.11**	0.7	2063.28	1072.17
	Water	3.8	0.053	5.11	1.23	0.47	0.6	**9.84**	21.103	11.263
	Total	1454.52	28.4	1420.15	885.77	749.62	2102.86	23.1	6665.42	–
	Gains	1080.67	27.35	776.64	437.334	319.11	1111.75	13.265	–	–
To	2022	Bare land	Built -up area	Farmland	Forest	Grassland	Shrubland	Water	Total	Loss
From 2001	Bare land	**316.61**	7.35	616.94	14.73	320.06	173.8	5.47	1454.96	1138.35
	Built-up area	0.9	**5.15**	15.907	0.8	1.023	4.51	0.165	28.46	23.3
	Farmland	27.8	41.26	**1085.35**	25.7	23.93	212.408	4.311	1420.76	335.37
	Forest	65.45	2.47	331.63	**184.82**	23.6	275	2.97	885.96	701.12
	Grassland	38.07	19.256	421.4	2.433	**153.06**	115.5	0.25	749.976	596.87
	Shrubland	98.617	19.14	1259.21	93.001	64.8	**567.77**	0.98	2103.52	1535.76
	Water	0.97	0.6	5.309	0.644	1.86	1.96	**10.55**	21.89	11.34
	Total	548.417	95.232	3735.753	322.13	588.34	1350.948	24.70	6665.42	–
	Gains	231.80	90.08	2650.403	137.30	435.3	783.178	14.15	–	–
To	2022	Bare land	Built-up area	Farmland	Forest	Grassland	Shrubland	Water	Total	Loss
From 1984	Bare land	**204.4**	7.352	258.5	15.156	161.4	115.5	3.78	766.08	561.68
	Built-up area	0.32	**1.936**	12.17	0.317	0.5	4.522	0.03	15	17.86
	Farmland	38.14	40.774	**954.1**	32.88	17.46	205.9	3.84	731.46	339
	Forest	53.00	4.1	432.17	**186.2**	16.9	270.24	3.99	873.83	780.4
	Grassland	121.00	22.53	881.75	11.25	**264.3**	233.17	0.83	2001.622	1270.54
	Shrubland	130.43	18.33	1191.9	75.7	127.25	**519**	1.32	2820.71	1544.94
	Water	1.1	0.2	5.17	0.6	0.6	2.547	**10.911**	24.44	10.21
	Total	548.41	95.23	3735.75	322.1	588.4	1351.	24.71	6665.42	–
	Gains	344.01	93.3	2781.66	135.91	324.08	831.87	13.8	–	–

accuracy. The model sensitivity result based on the ''forcing a single independent variable to be constant'' approach shows that keeping Var.8 constant reduces the model's accuracy by 79.79% and the skill measure by 0.59. Following evidence likelihood (Var.8), Var.5, Var.7, and Var.4 (Table 6) were the second, third, and fourth most important drivers of LULC change in the study area, respectively. On the other hand, Var.2, Var. 1, and Var. 3 were the first, second, and third least influential drivers of LULC dynamics. ''Forcing all independent variables except one to be constant'' and ''backward stepwise constant forcing'' sensitivity analysis models also demonstrated that variables 8 and 5 remain important factors for model performance (Tables 6 and 7) (see Table 8).

3.5. Model validation

A LULC map of 2022 was predicted using data from 1984 to 2001, and the model's accuracy was validated using the classified LULC map of 2022 through the Land Change Modeler (LCM). The results of K indices, such as Kno, Klocation, Klocationstrata, and Kstandard, had values of 90.39%, 88.12%, 89.12%, and 88.07%, respectively. Further analysis was done on the values of agreement and

Fig. 5. Contributors to net change in Built-up area (**a**), Shrubland (**b**), Farmland (**c**), Forest (**d**), Grassland (**e**), and Bare land (**f**) between 1984 and 2022.

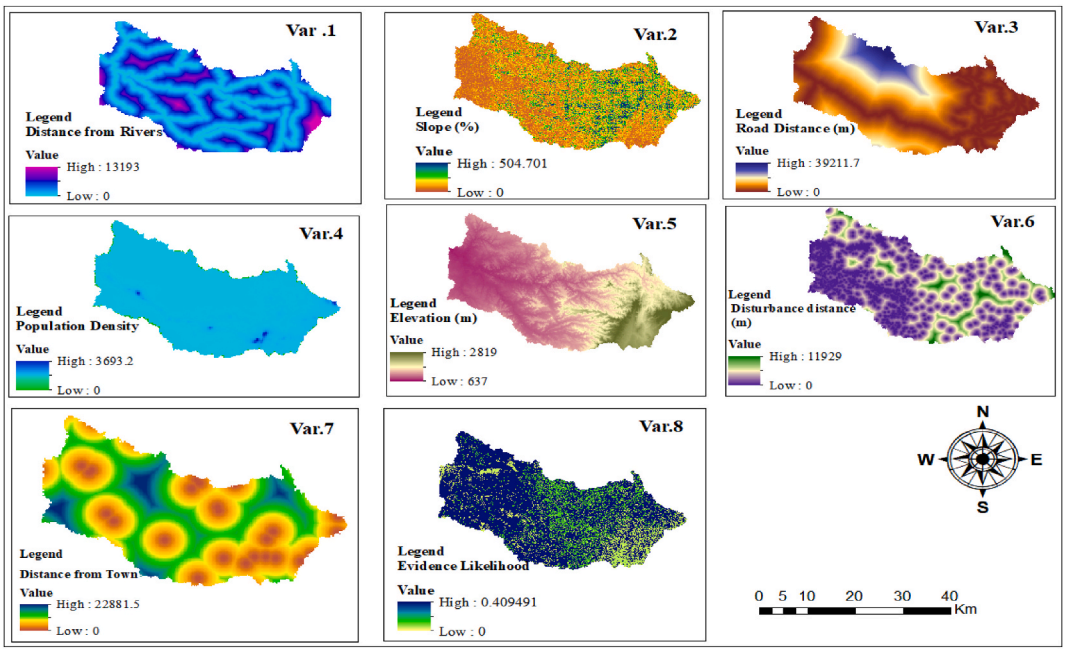

Fig. 6. Spatial driver variables; Var.1:Distance from rivers, Var.2:Slope, Var.3: Distance from roads, Var.4:Population density, Var.5:Elevation, Var.6: Distance from disturbance, Var.7:Distance from towns, and Var.8: Evidence likelihood.

Table 5
Model parameters and performance.

Explanatory variables	Variable description	Parameters and their performance	
Var. 1	Proximity from rivers and streams	Input layer neurons	8
Var. 2	Slope gradient	Hidden layer neurons	12
Var. 3	Proximity from road networks	Output layer neurons	14
Var. 4	Population density	Requested sample per class	1656
Var. 5	Elevation	Final learning rate	0.001
Var. 6	Distance from disturbance	Momentum factor	0.5
Var. 7	Distance from towns	Sigmoid constant	1
Var. 8	Evidence likelihood	Acceptable RMS	0.01
		Iteration	10,000
		Training RMS	0.28
		Testing RMS	0.0.31
		Accuracy rate	87.23%
		Skill measure	0.74

Table 6
Forcing a single independent variable to be constant and forcing all independent variables except one to be constant.

Forcing a single independent variable to be constant				Forcing all independent variables except one to be constant		
Model	Accuracy (%)	Skill measure	Influence order	Model	Accuracy (%)	Skill measure
With all variables	87.23	0.74	N/A	With all variables	87.23	0.744
Var. 1 constant	87.23	0.74	6	All constant but var. 1	50.89	0.017
Var. 2 constant	87.35	0.74	7	All constant but var. 2	50.89	0.017
Var. 3 constant	84.87	0.70	5	All constant but var. 3	51.95	0.040
Var. 4 constant	84.57	0.70	4	All constant but var. 4	50.89	**0.0177**
Var. 5 constant	81.44	0.63	2	All constant but var. 5	67.43	0.35
Var. 6 constant	87.41	0.75	8 (least influential)	All constant but var. 6	50.89	0.017
Var. 7 constant	82.80	0.65	3	All constant but var. 7	58.33	0.16
Var. 8 constant	79.79	0.59	1 (most influential)	All constant but var. 8	76.65	0.53

Table 7
Backwards stepwise constant forcing.

Model	Variables included	Accuracy (%)	Skill measure
With all variables	All variables	87.23	0.74
Step 1: var. [6] constant	[1,2,3,4,5,7,8]	87.41	0.75
Step 2: var. [6,1] constant	[2,3,4,5,7,8]	87.41	0.75
Step 3: var. [6,1,2] constant	[3,4,5,7,8]	87.29	0.74
Step 4: var. [6,1,2,3] constant	[4,5,7,8]	85.05	0.70
Step 5: var. [6,1,2,3,4] constant	[5,7,8]	82.62	0.65
Step 6: var. [6,1,2,3,4,5] constant	[7,8]	81.86	0.64
Step 7: var. [6,1,2,3,4,5,7] constant	[8]	76.65	0.53

disagreement. Accordingly, results for agreement chance, agreement quantity, agreement grid cell, and agreement quantity were found to be 0.125, 0.041, 0.047, 0.015, and 0.067, respectively.

3.5.1. Cramer's V coefficient of driver variables

Cramer's V coefficient was used to test the significance of the driver factors during the future LULC change prediction. The result of Cramer's V coefficient of the driver variables is presented in (Appendix Table B1). This study result signifies that elevation, population density, and evidence likelihood were the most critical driver variables to predict the future LULC transformations, while slope and proximity from rivers were the least important.

3.6. Prediction of future LULC change

The projected LULC map of 2040 and 2060 can be seen in Fig. 7. The findings revealed that farmland will increase by 23% between 2022 and 2040 and 31% between 2022 and 2060 (Table 9). Between 2040 and 2060, farmland is anticipated to expand at an annual rate of 48.8 km^2/yr^{-1} and 15.5 km^2/yr^{-1}, respectively. On the other hand, forest, grassland, and barren land will continue to decline significantly.

The future LULC analysis result in terms of net change, gains, and loss was also quantified as illustrated in Fig. 8a–b. The result indicated that grassland, forest and shrubland are expected to decline with net change of 426.37 km^2, 259.8 km^2 and 20.9 km^2, respectively (Fig. 8**a**), while farmland will show net increase of 1188.3 km^2 and gains of 1819.64 km^2 (Table 9 and Fig. 8b).

Table 8
Markovian transition probability matrix.

To	2001	Built-up area	Farmland	Bare land	Shrubland	Water	Forest	Grassland	*P*-year*
From 1984	Built-up area	0.0118	0.361	0.139	0.295	0.0038	0.06	0.1292	**2022**
	Farmland	0.007	0.4001	0.104	0.335	0.0038	0.09	0.0603	
	Bare land	0.0034	0.1267	0.404	0.206	0.0063	0.095	0.1586	
	Shrubland	0.0034	0.1788	0.219	0.395	0.0009	0.13	0.0724	
	Water	0.0037	0.2772	0.197	0.064	0.3484	0.07	0.0398	
	Forest	0.0026	0.1257	0.109	0.385	0.0007	0.357	0.0207	
	Grassland	0.0046	0.1993	0.339	0.212	0.0024	0.051	0.1915	
To	2022	Built-up area	Farmland	Bare land	Shrubland	Water	Forest	Grassland	
From 2001	Built-up area	0.2086	0.5363	0.031	0.156	0.0057	0.027	0.0358	**2040**
	Farmland	0.0289	0.774	0.018	0.145	0.0028	0.017	0.0149	
	Bare land	0.0019	0.3851	0.248	0.111	0.0037	0.009	0.2419	
	Shrubland	0.0064	0.5821	0.048	0.287	0.0001	0.046	0.0294	
	Water	0.027	0.2062	0.043	0.081	0.528	0.029	0.0856	
	Forest	0.0005	0.3298	0.077	0.328	0.0033	0.238	0.0226	
	Grassland	0.0252	0.5386	0.053	0.151	0.000	0.000	0.2324	
To	2022	Built-up area	Farmland	Bare land	Shrubland	Water	Forest	Grassland	
From 2001	Built-up area	0.0576	0.6626	0.0352	0.1734	0.0059	0.0287	0.0367	**2060**
	Farmland	0.0297	0.718	0.0286	0.169	0.004	0.0249	0.0259	
	Bare land	0.0197	0.6026	0.0819	0.157	0.004	0.0168	0.1178	
	Shrubland	0.0215	0.6736	0.0407	0.1912	0.0023	0.034	0.0368	
	Water	0.0286	0.4187	0.0482	0.1302	0.2632	0.0305	0.0807	
	Forest	0.0138	0.5792	0.0584	0.2274	0.0038	0.018	0.044	
	Grassland	**0.0278**	**0.6674**	**0.042**	**0.1671**	**0.002**	**0.0733**	**0.0756**	

P-year*: Prediction year.

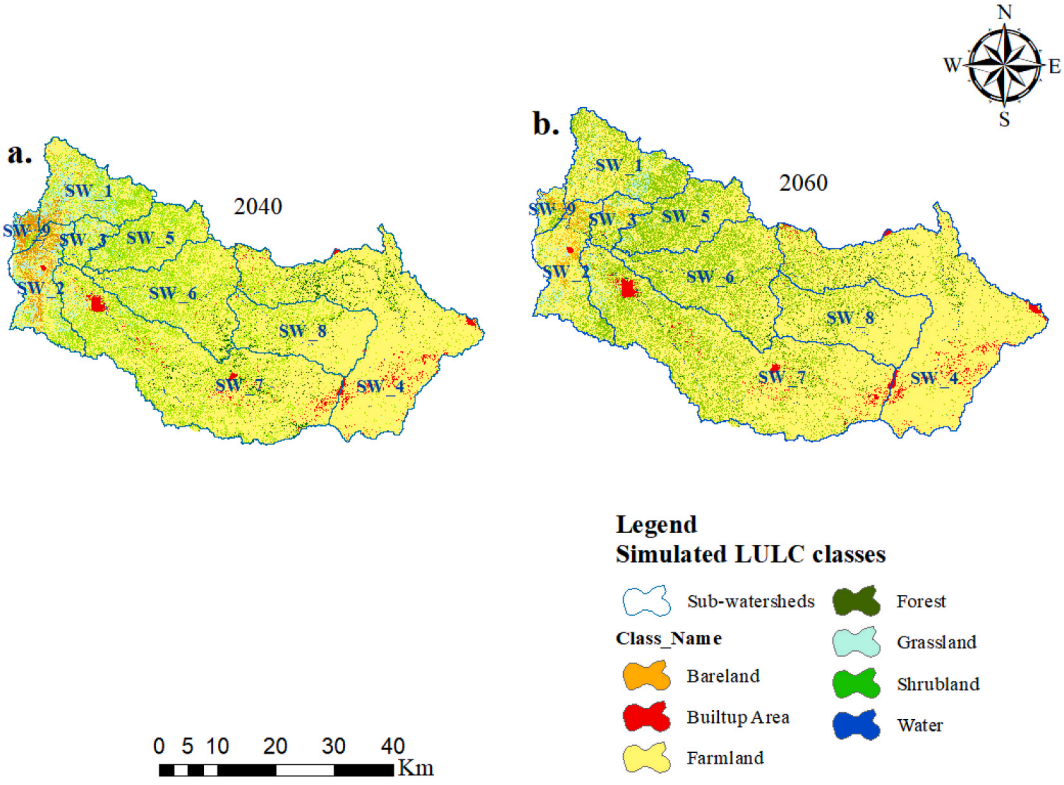

Fig. 7. Simulated LULC map; 2040 (**a**), 2060 (**b**), SW_1 (sub-watershed 1), SW_2 (sub-watershed 2), SW_3 (sub-watershed 3), SW_4 (sub-watershed 4), SW_5 (sub-watershed 5), SW_6 (sub-watershed 6), SW_7 (sub-watershed 7), SW_8 (sub-watershed 8), and SW_9 (sub-watershed 9).

Sub-watershed level changes in land cover, primarily in terms of forest, were detected in the study area to get a preliminary knowledge of the problem and to prioritize sub-watersheds during natural resource conservation planning. The findings suggest that during the predicted period of 2040, sub-watersheds 4, 7, and 8 would have 46.9 km^2, 38.7 km^2, and 12.9 km^2 of forest, respectively. In

Table 9
Actual area coverage and rates of LULC changes between 2022 and 2060 periods.

LULC class	Study periods						Annual rate of change (Km^2/year)					
	2022		2040		2060		2022–2040		2040–2060		2022–2060	
	Km^2	%	Km^2	%	Km^2	%	Km^2	Rate	Km^2	Rate	Km^2	Rate
Bare land	548.4	8.23	143.57	2.154	67.23	1.00	−404.83	−22.50	−76.33	−24.05	−481.16	−15.03
Built-up area	95.23	1.43	95.23	1.43	95.23	1.43	0	0	0	0	0	0
Farmland	3735.76	56.05	4613.97	69.22	4924.05	73.87	878.21	48.8	310.08	15.5	1188.2	31.27
Forest	322.1	4.83	110.09	1.65	62.3	0.93	−212.01	−11.78	−47.8	−2.39	−259.8	−6.83
Grassland	588.35	8.82	315.22	4.73	161.97	2.43	−273.12	−15.17	−153.25	−7.66	−426.37	−11.22
Shrubland	1350.86	20.27	1362.62	20.44	1329.92	19.95	11.76	0.65	−32.7	−1.63	−20.94	−0.55
Water	24.71	0.37	24.71	0.37	24.71	0.37	0	0	0		0	0
Total	6665.42	100	6665.42	100	6665.42	100						

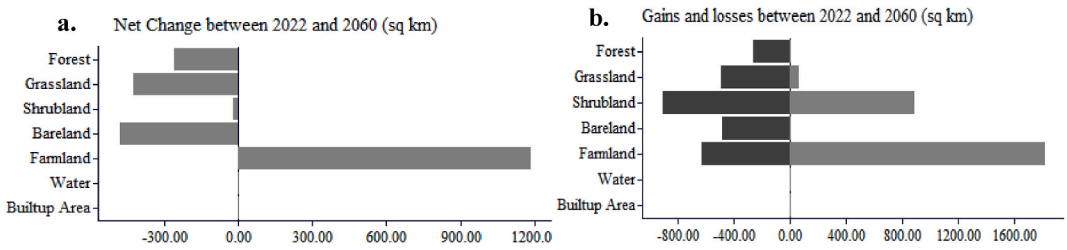

Fig. 8. Projected net change (**a**), gains, and loses (**b**) of LULC between 2022 and 2060 (Km^2).

contrast, sub-watersheds 1, 2, 3, 9, and 5 are expected to have the least amount of forest cover (Fig. 7**a** and **b**). Similarly, while the remaining sub-watersheds are likely to have less than 1 km^2 of forest cover, sub-watersheds 5, 7, 8, and 6 are expected to have the majority of the residual forest by 2060, sharing 25.3 km^2, 17 km^2, 13.3 km^2, and 6.4 km^2, respectively. However, it is vital to remember that, although other factors remain constant, the size of the sub-watershed will influence the ranges of amounts and sizes of forest cover.

4. Discussion

4.1. Accuracy assessment and LULC classification result

LULC classification results derived from remotely sensed satellite images will not be free of flaws and bias because the mapping process involves generalization [62,63]. Therefore, evaluating the accuracy of the satellite image classification result is crucial to determine its suitability for post-classification analysis and to comprehend the error and its likely implications [63]. This study attained an overall accuracy of 86.88%, 89.01%, and 92.95%, and Kappa values of 84.68%, 87.17%, and 91.76% for 1984, 2001, and 2022, respectively. The higher accuracy result of the 2022 image is due to the higher spatial resolution of sentinel-2A images vs. Landsat satellite images [19]. Overall, the accuracy assessment result of this study was above the specified levels of the relative strength of agreement as proposed by Landis and Koch [67].

Over the last 38 years, marked changes in LULC were detected in the Goang watershed, mainly in farmland, forest, shrubland, and grassland (and Fig. 4). During the 1984–2001 period, grassland experienced the most significant decline; i.e., 23% in 1984 vs. 11% in 2001. This result is also corroborated by KIs, who observed that between 1984 and 2001, flat slope areas with a predominance of grass and bushes were the first destinations targeted by migrant farmers to cultivate cash crops like Sesame (*Sesamum indicum* L) and Cotton (*Gossypium*) mainly in the lowland parts of the study area. This is because these areas were fertile and required less time and labor to prepare the farm plots for plowing. The rate of forest loss has increased considerably since 2001. This is due to the high demand for arable land and the concurrent indiscriminate clearing of forests, primarily related to the expansion of large-scale agricultural investment and population pressure induced by the temporary and permanent influx of immigrant farmers due to government-sponsored resettlement programs. The then-military government of Ethiopia started this program in the 1980s to alleviate the problem of recurring food insecurity, ease overwhelming human and livestock pressure on natural resources, and promote environmental rehabilitation in drought-prone areas of the country [59]. According to Yeshineh et al. [68], 83,102 re-settler households and 927 investors engaged in farming activities and charcoal production in the northwest lowlands, with average land holding sizes of 11–1500 and 2.5 ha, respectively, all hurt forests' ability to regenerate due to high deforestation, seedling, and sapling mortality. This study result is consistent with studies by Abera [69] in the Chewaka district, Degife et al. [70] in the Gambella region, Roba et al. [71] in the Nansebo district, Mengist et al. [72] in the Kaffa biosphere reserve, and Betru et al. [73] in Asossa zone who demonstrated that significant areas of forest and shrubland have been converted to farmland mainly due to myriad of factors including farmland expansion, resettlement, and population growth.

Most significantly, due to the need to maintain food security for the rapidly expanding population, farmland expanded dramatically over the past three decades, taking up more than half of the study area. This result concurs with the earlier research conducted throughout Ethiopia [18,73–76]. Contrasting reports, however, have also been done by Refs. [24,26,27,77], who highlighted the promising improvement of forest and vegetation cover as a result of land restoration activities through reforestation and afforestation of Acacia Decurrens and Eucalyptus. In particular, a study conducted by Minta et al. [78] in Dendi-Jeldu in the central Ethiopian highlands found that plantation forests increased by 13.6% as a result of the extension of Eucalyptus plantations in response to low agronomic productivity. Moreover, Wondie et al. [26] in the Fagita Lokoma district and Hussien et al. [25] in the Abbay River basin both found that the increase in forest cover was primarily due to the country's green legacy initiative and the conversion of cropland to plantations. The discrepancy between the reports from the previous studies in Ethiopia could be ascribed to several management and legislative factors contributing to LULC change. While some policies and programs may contribute to unsustainable land use practices, others may promote more sustainable land use practices, such as agroforestry and conservation agriculture. For example, government policies and programs promoting agricultural intensification and expansion, such as the Agricultural Development Led Industrialization (ADLI) strategy, may drive the increase in farmland and the concomitant decline in forest, shrubland, and grassland cover [79]. On the other hand, the Ethiopian government has also launched several initiatives to promote sustainable land use practices, such as the Sustainable Land Management program, which aims to address land degradation and promote sustainable agriculture.

The study also revealed that despite its quick and dramatic growth, a sizable portion of farmland was converted to built-up areas. The expansion of urban areas has resulted in converting agricultural land to built-up areas, potentially reducing agricultural productivity and contributing to environmental degradation. In line with this, various authors [22,36] in Ethiopia [80], in Nigeria [81], in China, and [82] in Belgium also reported that urbanization has had a significant detrimental influence on agriculture areas. The rapid expansion of the built-up area was also supported by KIs, who observed the establishment and expansion of several towns, such as Kumer, Kokit, Lemelem Terara, Dase, and Markoka, mainly after the start of resettlement programs. According to the KIs, the growth and expansion of these towns are ascribed to government-sponsored resettlement programs; when people are resettled, they frequently demand new housing and infrastructure, which can lead to the construction of new settlements and eventually rise to urban centers. Furthermore, resettlement programs can lead to changes in land use patterns as people engage in new economic activities and adopt new lifestyles; i.e., if resettled individuals engage in commercial agriculture, this can lead to the development of new market towns to support the trade of agricultural products.

4.2. Model performance and prediction of future LULC changes

The model performance of the MLP neural networks is presented in Table 5. Eastman [48] stipulates that the accuracy rate must be at least 80% to accept the model training results and continue the prediction procedure. Nonetheless, in this study, the MLP neural network model training obtained an accuracy rate of 88.68%, which is beyond the acceptable percentage of rate of accuracy. The model validation result regarding K-indices and agreement/disagreement values also demonstrated the model's good performance in predicting the future LULC change. Baig et al. [83] argued that overall K-standard values should be greater than 70% to use the model for future LULC prediction. However, this study result achieved greater than 80%, implying a good agreement between the projected and actual LULC map. The statistics of agreement/disagreement values, notably the lowest values of the Disagreement Grid cell and Disagreement Quantity, revealed the model validation result could effectively forecast LULC changes.

The simulated LULC maps of 2040 and 2060 are presented in Table 9 and Fig. 8. The findings suggested that the Goang watershed will continue to experience considerable LULC transformations in the future unless quick land management initiatives are done. Farmland will grow by 23% between 2022 and 2040 and 31% between 2022 and 2060. The lowland section of the Goang watershed near the Sudanese border was supposed to be a "Green Wall" to prevent the Sahara Desert from extending south of the Ethiopian highlands [68]. However, residual forest resources are projected to be considerably diminished. This would have an impact on ecosystem services, as well as exacerbate soil erosion and biodiversity loss.

4.3. Implications of LULC change for Goang watershed

Changes in LULC are an inevitable and complex biophysical phenomenon that markedly affects all groups of ecosystem services (ESs) and functions [4]. The Goang watershed is home to a wide range of forests and plant species that are significant from both an ecological and economic standpoint. Particularly, *Boswellia papyrifera*, often known as frankincense trees, predominate the forests in the lowland section of the study area and are crucial to the survival of the local inhabitants [52]. According to data gathered from KIs, selling resin and incense products from frankincense trees is the main source of income for most households. The community locally called incense "white gold" to infer its high price and demand in domestic and international markets. These trees boost the overall value of degraded areas by supplying crucial ecosystem services [84]. They also act as plant covers, generate large amounts of biomass, preserve the soil, and offer shade. However, because of irresponsible practices and their conversion to farmland, these native forest resources are in danger of extinction and are only found in inaccessible locations [29]. KIs noticed that before 10–15 years ago, wild animals and birds like antelope, Guinea fowl, Cheetahs, Hyaenas, Jackals, Bushbucks, and Leopards were common in the study area. However, these wild animals have decreased due to the deliberate burning of forests and grasslands to get new cultivable land [68]. Thus, to prevent the anticipated loss of key ESs, suitable land resource utilization, and prompt conservation measures are required in the Goang watershed.

5. Conclusions

This study was conducted to comprehend the past and projected changes in LULC in the Goang watershed. An integrated approach combining GIS, remote sensing, and MLP-CA-MC model was used to achieve the desired objectives. Based on the results of our study, the Goang watershed has experienced significant LULC changes over the past few decades, with forest, shrubland, and grassland cover showing a dramatic decline. These changes are driven by farmland and built-up area expansion, primarily attributed to rapid population growth. This study also demonstrates the effectiveness of MLP and CAMC algorithms in predicting future LULC changes, and the findings suggest that farming will continue to increase significantly. At the same time, forest, shrubland, and grassland cover are expected to decline sharply. The growth of agricultural land at the expense of forest and shrub lands may eventually lead to soil erosion and degradation, increasing the susceptibility of the watershed to desertification, which will be challenging to reverse.

Based on our research results, we recommend policymakers take measures to address the underlying causes of LULC change in the Goang watershed. These measures include promoting sustainable land use practices, managing population growth, and protecting and restoring forested areas. Implementing such policies should be based on scientific evidence and should consider the complex interactions between ecological, social, and economic factors in the study area.

Although this study provides valuable insights into the dynamics of LULC in the Goang watershed, some limitations should be noted. While we used Landsat and Sentinel-2A satellite images, the resolution may not be sufficient to capture fine-scale LULC changes

that occur over short periods. Furthermore, though we used a variety of driver variables to improve the accuracy of our models, there may be other factors that influence LULC change that we should have considered.

Author contribution statement

Getahun Sisay: Conceived and designed the experiments; Performed the experiments; Analyzed and interpreted the data; Wrote the paper.

Berehan Gesesse: Christine Fürst: Meseret Kassie: Belaynesh Kebede: Conceived and designed the experiments; Analyzed and interpreted the data; Contributed reagents, materials, analysis tools or data; Wrote the paper

Funding statement

This research did not receive any specific grant from funding agencies in the public, commercial, or not-for-profit sectors.

Data availability statement

Data will be made available on request.

Additional information

No additional information is available for this paper.

Declaration of competing interest

The authors declare no competing interests.

Acknowledgments

We are grateful to the anonymous reviewers and the journal editor for their insightful remarks and helpful suggestions, which significantly improved the quality of this work. We would like to thank the University of Gondar for supporting the first author who is a Ph.D candidate. We would also want to thank the farmers and district experts for their cooperation during fieldwork and data collection.

Appendix A. Accuracy assessment result for historical LULC maps

Table A1Accuracy assessment result for the 1984 LULC map

	LULC	Bare land	Grassland	Farmland	Water	Forest	Shrubland	Built up Area	Row total	UA (%)
1984	Bare land	**65**	4	5	0	1	1	3	79	82.27848
	Grassland	4	**84**	4	0	3	5	0	100	84
	Farmland	4	1	**77**	0	1	2	0	85	90.6
	Water	1	2	0	**74**	0	0	0	77	96.10
	Forest	0	3	2	2	**76**	8	0	91	83.51
	Shrubland	1	2	4	1	7	**79**	1	95	83.15
	Built up Area	6	0	1	0	0	1	**75**	83	90.36
	Column total	81	96	93	77	88	96	79	610	
	PA (%)	80.24	87.5	82.8	96.10	86.36	82.3	94.93		
	Overall accuracy: 86.88 Kappa: 0.8468									

Table A2
Accuracy assessment result for the 2001 LULC map

	Class name	Bare land	Grassland	Farmland	Water	Forest	Shrubland	Built-up Area	Row total	UA (%)
2001	Bare land	**70**	2	8	1	1	2	3	87	80.46
	Grassland	1	**75**	3	2	2	4	2	89	84.27
	Farmland	5	0	**70**	0	0	2	0	77	90.90
	Water	2	2	1	**77**	0	0	1	83	92.77
	Forest	0	1	0	0	**74**	6	0	81	91.35
	Shrubland	2	1	0	1	3	**89**	0	96	92.70
	Built-up Area	7	0	1	0	1	0	**88**	97	90.70
	Column total	87	81	83	81	81	103	94	610	
	PA (%)	80.46	92.6	84.33	95.06	91.35	86.40	93.60		
	Overall accuracy: 89% Kappa:87%									

Table A3
Accuracy assessment result for 2022 LULC map

	Class name	Barren land	Grassland	Farmland	Water	Forest	Shrubland	Built up Area	Row total	UA
2022	Barren land	**88**	2	2	1	0	1	2	96	91.7
	Grassland	1	**81**	1	0	2	3	0	88	92.04
	Farmland	3	2	**70**	0	0	1	0	76	92.1
	Water	0	2	0	**80**	0	0	0	82	97.56
	Forest	0	0	0	0	**75**	4	0	79	94.93
	Shrubland	2	2	2	0	4	**85**	0	95	89.47
	Built up Area	4	0	0	0	0	2	**88**	94	93.61
	Column total	98	89	75	81	81	96	90	610	
	PA	89.8	91.01	93.4	98.76	92.6	88.5	97.8		
	Overall Accuracy: 92.95 Kappa coefficient: 0.91									

Appendix B

Table B1
Driver Variables and their Cramer's V and P value

S.no.	Driver variables	Type	Overall Cramer's V value	*P*-Value
1	Elevation	Static	0.2707	0.0000
2	Slope Gradient	Static	0.0872	0.0000
3	Proximity from Rivers and Streams	Dynamic	0.0585	0.0000
4	Proximity from Road networks	Dynamic	0.1337	0.0000
5	Proximity from Towns and Villages	Dynamic	0.1221	0.0000
6	Population Density	Dynamic	0.1562	0.0000
7	Evidence Likelihood	Dynamic	0.8452	0.0000
8	Distance from Disturbance	Dynamic	0.2114	0.0000

References

[1] E.F. Lambin, B.L. Turner, H.J. Geist, S.B. Agbola, A. Angelsen, J.W. Bruce, et al., The Causes of Land-Use and Land-Cover Change: Moving beyond the Myths, vol. 11, Global Environmental Change, 2001.
[2] K. Fuladlu, Thermal response to land-use land-cover patterns: an experimental study in famagusta, Cyprus. Clean (Weinh) 50 (9) (2022). Sep. 1.
[3] G. Duveiller, L. Caporaso, R. Abad-Viñas, L. Perugini, G. Grassi, A. Arneth, et al., Local biophysical effects of land use and land cover change: towards an assessment tool for policy makers, Land Use Pol. 91 (2020).
[4] E.F. Lambin, H. Geist, R.R. Rindfuss, Introduction: local processes with global impacts, in: Land-Use and Land-Cover Change, 2008.
[5] R. Makwinja, E. Kaunda, S. Mengistou, T. Alamirew, Impact of land use/land cover dynamics on ecosystem service value—a case from Lake Malombe, Southern Malawi, Environ. Monit. Assess. 193 (8) (2021).
[6] X.P. Song, M.C. Hansen, S.V. Stehman, P.V. Potapov, A. Tyukavina, E.F. Vermote, et al., Global land change from 1982 to 2016, Nature 560 (7720) (2018).
[7] Q. Wang, Q. Guan, J. Lin, H. Luo, Z. Tan, Y. Ma, Simulating land use/land cover change in an arid region with the coupling models, Ecol. Indicat. (2021) 122.
[8] P.G. Curtis, C.M. Slay, N.L. Harris, A. Tyukavina, M.C. Hansen, Classifying drivers of global forest loss, Science (1979) (6407) (2018) 361.
[9] A Al Kafy, A Al Faisal, R.M. Shuvo, M.N.H. Naim, M.S. Sikdar, R.R. Chowdhury, et al., Remote sensing approach to simulate the land use/land cover and seasonal land surface temperature change using machine learning algorithms in a fastest-growing megacity of Bangladesh, Remote Sens. Appl. (2021) 21.
[10] K. Winkler, R. Fuchs, M. Rounsevell, M. Herold, Global land use changes are four times greater than previously estimated, Nat. Commun. 12 (1) (2021).
[11] FAO, Global Forest Resources Assessment 2015, 2015. Rome.
[12] FAO and UNEP, The State of the World's Forests: Forest, Biodiversity and People, Rome Italy, Rome, 2020.
[13] T. Gashaw, T. Tulu, M. Argaw, A.W. Worqlul, Evaluation and prediction of land use/land cover changes in the Andassa watershed, Blue Nile Basin, Ethiopia, Environmental Systems Research 6 (1) (2017).
[14] C. Hyandye, L.W. Martz, A Markovian and cellular automata land-use change predictive model of the Usangu Catchment, Int. J. Rem. Sens. 38 (1) (2017).
[15] R.J. Keenan, G.A. Reams, F. Achard, J.V. de Freitas, A. Grainger, E. Lindquist, Dynamics of Global Forest Area: Results from the FAO Global Forest Resources Assessment 2015 vol. 352, Forest Ecology and Management, 2015.
[16] E.S.P. Assede, H. Orou, S.S.H. Biaou, C.J. Geldenhuys, F.C. Ahononga, P.W. Chirwa, Understanding drivers of land use and land cover change in africa, a review 8 (2023) 62–72.
[17] E. Nkonya, T. Johnson, H.Y. Kwon, E. Kato, Economics of land degradation in sub-Saharan Africa, in: Economics of Land Degradation and Improvement - A Global Assessment for Sustainable Development, 2015.
[18] T. Belay, D.A. Mengistu, Land use and land cover dynamics and drivers in the Muga watershed, Upper Blue Nile basin, Ethiopia, Remote Sens. Appl. 15 (2019).
[19] R. Girma, C. Fürst, A. Moges, Land use land cover change modeling by integrating artificial neural network with cellular Automata-Markov chain model in Gidabo river basin, main Ethiopian rift, Environmental Challenges 6 (2022).
[20] D.A. Malede, T. Alamirew, J.R. Kosgie, T.G. Andualem, Analysis of land use/land cover change trends over Birr River Watershed, Abbay Basin, Ethiopia, Environmental and Sustainability Indicators (2023 Feb 1) 17.
[21] G. Sisay, G. Gitima, M. Mersha, W.G. Alemu, Assessment of land use land cover dynamics and its drivers in bechet watershed upper blue nile basin, Ethiopia, Remote Sens. Appl. 24 (2021).
[22] T.D. Tasgara, B. Kumar, Assessment of land use/land cover change impact on streamflow: a case study over upper Guder Catchment, Ethiopia, Sustain Water Resour Manag 9 (1) (2023 Feb 1).
[23] W. Mengist, T. Soromessa, G.L. Feyisa, Estimating the total ecosystem services value of Eastern Afromontane Biodiversity Hotspots in response to landscape dynamics, Environmental and Sustainability Indicators (2022) 14.

[24] W. Bewket, Land cover dynamics since the 1950s in Chemoga watershed , Blue Nile basin, Ethiopia, Mt. Res. Dev. 22 (3) (2002).
[25] K. Hussien, A. Kebede, A. Mekuriaw, S. Asfaw Beza, S. Haile Erena, Modelling spatiotemporal trends of land use land cover dynamics in the Abbay River Basin, Ethiopia, Model Earth Syst, Environ 9 (2023) 347–376.
[26] M. Wondie, W. Mekuria, Planting of acacia decurrens and dynamics of land cover change in fagita lekoma district in the Northwestern Highlands of Ethiopia, Mt. Res. Dev. 38 (3) (2018).
[27] B. Zerga, B. Warkineh, D. Teketay, M. Woldetsadik, M. Sahle, Land use and land cover changes driven by expansion of eucalypt plantations in the Western Gurage Watersheds, Centeral-south Ethiopia, Trees, Forests and People 5 (2021).
[28] M.S. Regasa, M. Nones, D. Adeba, A review on land use and land cover change in ethiopian basins, Land 10 (6) (2021 Jun 1).
[29] M. Lemenih, H. Kassa, G.T. Kassie, D. Abebaw, W. Teka, Resettlement and woodland management problems and options: a case study from North-Western Ethiopia, Land Degrad. Dev. 25 (4) (2014).
[30] M. Mekonnen, T. Sewunet, M. Gebeyehu, B. Azene, A.M. Melesse, Gis and Remote Sensing-Based Forest Resource Assessment, Quantification, and Mapping in Amhara Region, Ethiopia, Springer Geography, 2016.
[31] M. Mekonnen, T. Sewunet, M. Gebeyehu, B. Azene, A.M. Melesse, Gis and Remote Sensing-Based Forest Resource Assessment, Quantification, and Mapping in Amhara Region, Ethiopia, Springer Geography, 2016.
[32] D. Abebaw, H. Kassa, G.T. Kassie, M. Lemenih, B. Campbell, W. Teka, Dry Forest-Based Livelihoods in Resettlement Areas of Northwestern Ethiopia, vol. 20, For Policy Econ, 2012.
[33] W. Zewdie, E. Csaplovics, L. Inostroza, Monitoring ecosystem dynamics in northwestern Ethiopia using NDVI and climate variables to assess long term trends in dryland vegetation variability, Appl. Geogr. 79 (2017 Feb 1) 167–178.
[34] B. Alemu, E. Garedew, Z. Eshetu, H. Kassa, Land use and land cover changes and associated driving forces in North western lowlands of Ethiopia, Int Res J Agric Sci Soil Sci 5 (1) (2015).
[35] ER da Cunha, C.A.G. Santos, RM da Silva, V.M. Bacani, A. Pott, Future scenarios based on a CA-Markov land use and land cover simulation model for a tropical humid basin in the Cerrado/Atlantic Forest ecotone of Brazil, Land Use Pol. (2021) 101.
[36] M.B. Fitawok, B. Derudder, A.S. Minale, S Van Passel, E. Adgo, J. Nyssen, Modeling the impact of urbanization on land-use change in Bahir Dar City, Ethiopia: an integrated cellular automata-Markov chain approach, Land 9 (4) (2020).
[37] E. Gidey, O. Dikinya, R. Sebego, E. Segosebe, A. Zenebe, Cellular automata and Markov chain (CA_Markov) model-based predictions of future land use and land cover scenarios (2015–2033) in Raya, northern Ethiopia, Model Earth Syst Environ 3 (4) (2017).
[38] A.L. Kura, D.L. Beyene, Cellular automata Markov chain model-based deforestation modelling in the pastoral and agro-pastoral areas of southern Ethiopia, Remote Sens. Appl. 18 (2020).
[39] G. Kust, O. Andreeva, A. Cowie, Land Degradation Neutrality: concept development, practical applications and assessment, J Environ Manage 195 (2017).
[40] A.L. Cowie, B.J. Orr, V.M. Castillo Sanchez, P. Chasek, N.D. Crossman, A. Erlewein, et al., Land in balance: the scientific conceptual framework for Land Degradation Neutrality, Environ Sci Policy 79 (2018).
[41] V.N. Mishra, P.K. Rai, A remote sensing aided multi-layer perceptron-Markov chain analysis for land use and land cover change prediction in Patna district (Bihar), India, Arabian J. Geosci. 9 (4) (2016).
[42] M.K. Leta, T.A. Demissie, J. Tränckner, Modeling and prediction of land use land cover change dynamics based on land change modeler (Lcm) in nashe watershed, upper blue nile basin, Ethiopia, Sustainability 13 (7) (2021).
[43] O.A. Zubair, W. Ji, T.E. Weilert, Modeling the impact of urban landscape change on urban wetlands using similarityweighted instance-based machine learning and Markov model, Sustainability 9 (12) (2017).
[44] M. Asempah, W. Sahwan, B. Schütt, Assessment of land cover dynamics and drivers of urban expansion using geospatial and logistic regression approach in wa municipality, Ghana, Land 10 (11) (2021).
[45] S. Saadani, R. Laajaj, M. Maanan, H. Rhinane, A. Aaroud, Simulating spatial–temporal urban growth of a Moroccan metropolitan using CA–Markov model, Spatial Information Research 28 (5) (2020).
[46] R. Hamad, H. Balzter, K. Kolo, Predicting land use/land cover changes using a CA-Markov model under two different scenarios, Sustainability 10 (10) (2018).
[47] A. Gharaibeh, A. Shaamala, R. Obeidat, S. Al-Kofahi, Improving land-use change modeling by integrating ANN with Cellular Automata-Markov chain model, Heliyon 6 (9) (2020).
[48] J.R. Eastman, TerrSet Geospational Monitoring and Modeling System, 2016. www.clarklabs.org.
[49] H. Hurni, Agroecological belts of Ethiopia, in: Explanatory Notes on Three Maps at a Scale of 1, vol. 1, 1998.
[50] M. Tekleyohannes, B. Grum, N. Abebe, B.A. Abebe, Optimization of rain gauge network using multi-criteria decision analysis and entropy approaches: case of Tekeze River basin, northwestern Ethiopia, Theor. Appl. Climatol. 145 (1–2) (2021).
[51] A. Wassie, Forest Resources in Amhara: Brief Description, Distribution and Status, 2017.
[52] A. Eshete, D. Teketay, M. Lemenih, F. Bongers, Effects of resin tapping and tree size on the purity, germination and storage behavior of Boswellia papyrifera (Del.) Hochst. seeds from Metema District, northwestern Ethiopia, For Ecol Manage 269 (2012).
[53] Atlanta Satellite Facility, High-resolution Advanced Land Observing Satellite-Phased Array-Type-L-Nand Synthetic Aperture Radar (ALOS-PALASAR) Radiometric Terrain Corrected (RTC) DEM, 2022. Aug 24]. Available from: https://asf.alaska.edu.
[54] Worldpop, Global High-Resolution Population Denominators Project, 2018 [cited 2023 Aug 24]. Available from: www.worldpop.org.
[55] R.G. Congalton, A comparison of sampling schemes used in generating error matrices for assessing the accuracy of maps generated from remotely sensed data, Photogramm Eng Remote Sensing 54 (5) (1988).
[56] B. Gessesse, W. Bewket, A. Bräuning, Land use and land cover transformation and its implication on land degradation: the case of Modjo watershed, Ethiopia, in: Extreme Hydrology and Climate Variability: Monitoring, Modelling, Adaptation and Mitigation, 2019.
[57] G. Gitima, M. Teshome, M. Kassie, M. Jakubus, Spatiotemporal land use and cover changes across agroecologies and slope gradients using geospatial technologies in Zoa watershed, Southwest Ethiopia, Heliyon 8 (9) (2022 Sep 1).
[58] K. Xu, Q. Tian, Y. Yang, J. Yue, S. Tang, How up-scaling of remote-sensing images affects land-cover classification by comparison with multiscale satellite images, Int. J. Rem. Sens. 40 (7) (2019).
[59] K. Belay, Resettlement of peasants in Ethiopia, Journal of Rural Development/Nongchon-Gyeongje. 27 (4) (2004).
[60] T. Kassawmar, S. Eckert, K. Hurni, G. Zeleke, H. Hurni, Reducing landscape heterogeneity for improved land use and land cover (LULC) classification across the large and complex Ethiopian highlands, Geocarto Int. 33 (1) (2018).
[61] G.W. Woldemariam, D. Tibebe, T.E. Mengesha, T.B. Gelete, Machine-learning algorithms for land use dynamics in Lake Haramaya Watershed, Ethiopia, Model Earth Syst Environ 8 (2022) 3719–3736.
[62] R.G. Congalton, K. Green, Assessing the accuracy of remotely sensed data: principles and practices, in: Assessing the Accuracy of Remotely Sensed Data: Principles and Practices, second ed., 2008. Second Edition.
[63] G.M. Foody, Status of Land Cover Classification Accuracy Assessment, vol. 80, Remote Sensing of Environment, 2002.
[64] A. Arora, M. Pandey, V.N. Mishra, R. Kumar, P.K. Rai, R. Costache, et al., Comparative evaluation of geospatial scenario-based land change simulation models using landscape metrics, Ecol. Indicat. (2021) 128.
[65] Q. Wang, Q. Guan, J. Lin, H. Luo, Z. Tan, Y. Ma, Simulating land use/land cover change in an arid region with the coupling models, Ecol. Indicat. (2021) 122.
[66] W.T. Dibaba, T.A. Demissie, K. Miegel, Watershed hydrological response to combined land use/land cover and climate change in highland Ethiopia: finchaa catchment, Water (Switzerland) 12 (6) (2020).
[67] A.J. Viera, J.M. Garrett, Understanding interobserver agreement: the kappa statistic, Fam. Med. 37 (5) (2005).
[68] G. Yeshineh, M. Mekonnen, G. Zeleke, G. Desta, Threats and management options of the green belt natural forest, northwest lowlands of Ethiopia, Trees, Forests and People (2022 Sep 1) 9.

[69] A. Abera, T. Yirgu, A. Uncha, Impact of resettlement scheme on vegetation cover and its implications on conservation in Chewaka district of Ethiopia, Environmental Systems Research 9 (1) (2020).
[70] A.W. Degife, F. Zabel, W. Mauser, Assessing land use and land cover changes and agricultural farmland expansions in Gambella Region, Ethiopia, using Landsat 5 and Sentinel 2a multispectral data, Heliyon 4 (11) (2018).
[71] I.L. Roba, E.E. Dube, D.L. Beyene, Resettlement and its Impacts on Land Use Land Cover Change in Nansebo District, Ethiopia, GeoJournal, 2021.
[72] W. Mengist, T. Soromessa, G.L. Feyisa, Monitoring Afromontane Forest cover loss and the associated socio-ecological drivers in Kaffa biosphere reserve, Ethiopia, Trees, Forests and People 6 (2021).
[73] T. Betru, M. Tolera, K. Sahle, H. Kassa, Trends and drivers of land use/land cover change in Western Ethiopia, Appl. Geogr. 104 (2019).
[74] G. Abebe, D. Getachew, A. Ewunetu, Analysing land use/land cover changes and its dynamics using remote sensing and GIS in Gubalafito district, Northeastern Ethiopia, SN Appl. Sci. 4 (1) (2022).
[75] T.T. Muleta, M. Kidane, A. Bezie, The effect of land use/land cover change on ecosystem services values of Jibat forest landscape, Ethiopia, Geojournal 86 (5) (2021).
[76] S. Tadese, T. Soromessa, T. Bekele, Analysis of the current and future prediction of land use/land cover change using remote sensing and the CA-markov model in majang forest biosphere reserves of Gambella, southwestern Ethiopia, Sci. World J. (2021) 2021.
[77] F. Alemayehu, N. Taha, J. Nyssen, A. Girma, A. Zenebe, M. Behailu, et al., The impacts of watershed management on land use and land cover dynamics in Eastern Tigray (Ethiopia), Resour. Conserv. Recycl. 53 (4) (2009).
[78] M. Minta, K. Kibret, P. Thorne, T. Nigussie, L. Nigatu, Land use and land cover dynamics in Dendi-Jeldu hilly-mountainous areas in the central Ethiopian highlands, Geoderma (2018) 314.
[79] M. Biedemariam, E. Birhane, B. Demissie, T. Tadesse, G. Gebresamuel, S. Habtu, Ecosystem service values as related to land use and land cover changes in Ethiopia, A Review 11 (2022). Land.
[80] M.Y. Onanuga, A.O. Eludoyin, I.E. Ofoezie, Urbanization and its effects on land and water resources in Ijebuland, southwestern Nigeria, Environ. Dev. Sustain. 24 (1) (2022).
[81] Z. Huang, X. Du, C.S.Z. Castillo, How does urbanization affect farmland protection? Evidence from China, Resour. Conserv. Recycl. 145 (2019).
[82] V. Beckers, L. Poelmans, A. Van Rompaey, N. Dendoncker, The impact of urbanization on agricultural dynamics: a case study in Belgium, J. Land Use Sci. 15 (5) (2020).
[83] M.F. Baig, M.R.U. Mustafa, I. Baig, H.B. Takaijudin, M.T. Zeshan, Assessment of land use land cover changes and future predictions using CA-ANN simulation for selangor, Malaysia, Water (Switzerland) 14 (3) (2022).
[84] K. Gebrehiwot, B. Muys, M. Haile, R. Mitloehner, Introducing Boswellia papyrifera (Del.) Hochst and its non-timber forest product, frankincense, Int. For. Rev. 5 (4) (2003).